Table 1

Aerofoil	M_∞	χ	x_s	$\epsilon(\chi)$
NACA 0012[a]	0.902	−0.476	0.895	1.56
NACA 0012[b]	0.864	−0.676	0.675	1.50
NACA 0012[c]	0.815	−0.952	0.49	1.45
NACA 0012[c]	0.791	−1.093	0.39	1.43
NACA 0015[a]	0.81	−0.84	0.56	1.48
6% Circular arc[d]	0.909	−0.699	0.84	1.43
6% Circular arc[d]	0.872	−1.01	0.735	1.35

[a]Example quoted in Ref. 3.
[b]Example quoted in Ref. 4.
[c]Examples calculated by the Aircraft Research Association.
[d]Example quoted in Ref. 2.
Values of $\epsilon(\chi)$ for Several Test Cases.

ahead of the shock is given fairly accurately by the method of Ref. 1; this implies that the functional dependence of $g(x,x_s)$ on x is adequately represented by $I[x,x_s,\bar{U}(x,o)]$.

From the similarity laws regarding the transonic flow around affinely related thin aerofoils the velocity distribution $\bar{U}(x,o)$ should remain unchanged provided the transonic similarity parameter, χ, given by

$$\chi = -\frac{(1-M_\infty^2)}{(k\tau)^{2/3}} \tag{12}$$

where τ is the thickness parameter of the aerofoil, remains constant. If χ is unchanged then $\bar{Z}_T''(x)$ is unchanged and hence $I[x,x_s,\bar{U}(x,o)]$, given by Eq. (7), is unchanged. Furthermore to first order in the thickness parameter $\bar{U}_{TL}(x)$ is unchanged and hence it can be implied that ϵ is a function of the similarity parameter χ. The correction factor, ϵ, may also be a function of additional parameters that characterise a particular family of aerofoils but as a first step it is assumed in this analysis that ϵ is a function only of χ. Thus

$$\epsilon = \epsilon(x) \tag{13}$$

Since it has been assumed earlier that $\epsilon(\chi)$ is independent of the chordwise variable it is implied by Eq. (13) that $\epsilon(\chi)$ is the same function of χ whatever the aerofoil under consideration. The main discrepancy in the result of Ref. 1 is in the shock location and it is proposed to find $\epsilon(\chi)$ by reference to the more exact numerical results[2-4] now available to locate the shock wave accurately in a number of examples.

Results

In the results of the numerical methods of Refs. 2-4 the shock wave is represented by a rapid compression and for the present purpose it is assumed that the shock wave lies at the midpoint of this rapid compression.

Seven examples are used and details of the aerofoils and the origin of the data as well as the calculated values of $\epsilon(\chi)$ are given in Table 1.

It is desirable to approximate the correction factor $\epsilon(\chi)$ by some analytic function of χ and this is done by representing $\epsilon(\chi)$ by a second order polynomial in χ and correlating the shock locations to minimise the percentage error; $\epsilon(\chi)$ is found to be given approximately by

$$\epsilon(x) \approx 1.614 + 0.178x + 0.0095x^2 \tag{14}$$

This approximation to $\epsilon(\chi)$ correlates the shock locations in the seven examples to an accuracy of 3%. It is interesting to note that the variation of $\epsilon(\chi)$ with χ is relatively small.

Having located the shock wave fairly accurately the corresponding pressure (or velocity) distributions can be determined.

The pressure distribution (p/p_o), where p_o is the stagnation pressure, for the flow around a NACA 0012 aerofoil at $M_\infty = 0.864$ (one of the seven examples) is shown in Fig. 2 and is compared to the pressure distribution found by Steger and Lomax.[4] The present results compare favourably with those of Steger and Lomax except in the immediate vicinity of the shock where the pre-shock compression and the post-shock expansion predicted by Oswatitsch and Zierup[5] is evident.

In addition the velocity distribution $\bar{U}(x,o)$ over the 6% circular arc aerofoil at $M_\infty = 0.872$ has been calculated and is shown in Fig. 1 for comparison with the results of Ref. 1 and Ref. 2. The present results compare well with those found by Murman and Cole[2] ahead of the shock wave but behind the shock there is substantial disagreement. The reason for this disagreement is not clear but at least the present results give the correct shock jump relations.

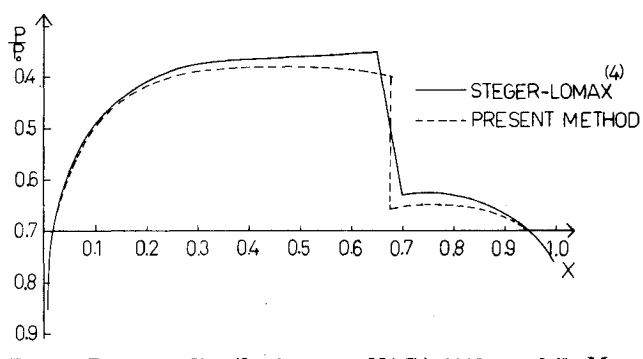

Fig. 2 Pressure distribution on a NACA 0012 aerofoil; M_∞ = 0.864

References

[1]Spreiter, J. R. and Alksne, A., "Theoretical Prediction of Pressure Distributions on Non-Lifting Airfoils at High Subsonic Speeds," TN 3096, 1954, NACA.

[2]Murman, E. and Cole, J. D., "Calculation of Plane Steady Transonic Flows," *AIAA Journal*, Vol. 9, No. 1, Jan. 1971. pp. 114-121.

[3]Murman, E., "Computational Methods for Inviscid Transonic Flows with Imbedded Shock Waves," *Numerical Methods in Fluid Dynamics*—AGARD LS-48 1972, Chap. 13.

[4]Steger, J. L. and Lomax, H., "Numerical Calculation of Transonic Flows about Two-Dimensional Airfoils by Relaxation Procedures," AIAA Paper 71-569 June 1971,

[5]Oswatitsch, K. and Zierup, J., "Das Problem des senkrechten stosses an einer gekrummten Wand," Zeitschrift fur Angewandt Mathematik und Mechanik, Vol. 40 1960, pp. 143-144.

[6]Nixon, D. and Hancock, G. J., "High Subsonic Flow Past a Two-Dimensional Aerofoil," Rept. QMC-EP 1000 1972, Queen Mary College, London, England.

An Optimized Video Output from a Wide Angle Optical Probe

J. A. Mays* and R. E. Holmes†
Systems Research Laboratories, Inc., Dayton, Ohio

THE current and future requirements for Aircraft/Aerospace Visual Simulators demands ever increasing resolution. This is necessary in order that existing simulation

Submitted as Paper 73-918 at the AIAA Visual and Motion Simulation Conference, Palo Alto, Calif., September 10-12, 1973; received September 26, 1973; revision received November 26, 1973. Acknowledgement is made to Mr. C. F. McNulty, Chief of the Simuationa Techniques Branch, Air Force Human Resources Laboratory, WPAFB, Dayton, Ohio, and to Mr. A. T. Gill, Contract Monitor, for their assistance, cooperation, and consultation throughout the program.

Index categories: Aircraft Crew Training; Spacecraft Ground Testing and Simulation (Including Components).

*Staff Video Engineer, Electronic Image Systems Group.
†Manager Electronic Image Systems Group.

displays utilizing 45 to 60° fields of view, may be upgraded and to maintain or improve the visual acuity of displays with 110° and greater fields of view. Existing optical probe/television camera visual simulation image generators typically exhibit narrow fields of view, and picture degradation occurs at low simulated altitudes.

Two fundamental problem areas have contributed to this situation: 1) field of view and depth of field limitations in the optical probe; and 2) resolution limitations of television cameras. The Air Force has already accomplished a solution to the former problem area by means of a previous development program which resulted in a wide-angle infinite depth of focus optical probe. The objectives of the work being reported here were to conduct a research program to achieve an optimized video output from a government furnished optical probe. The primary goal was to investigate: 1) model paints, textures and illumination sources; 2) optical probe resolution, spectral response, and mapping functions; and 3) TV camera/intensifier spectral response, gain, resolution and distortion. A TV camera capable of 2000 TVL horizontal and 1000 TVL vertical resolution was developed to interface with the optical probe.

Analysis of the Optical Probe

The optical probe utilized in the program was manufactured by the Farrand Optical Co. and is described in an Air Force technical report.[1] Although the technical report on the optical probe was rather complete, several tests were performed to check the data and to become familiar with its operation. The parameters measured in this study were field of view, distortion, optical resolution, and spectral response. As a supplement to the probe's technical report, spectral response data was also taken to aid in the selection of lighting and model characteristics for an optimum video system. The results of these tests indicated that the probe sharply attenuates the blue and actually peaks at 625 nanometers. The relative response was found to be 50% at 500 nanometers and 10% at 450 nanometers.

Optical Probe and Vidicon Interfacing Technique

The image diameter at the output of the probe is only 16 mm, therefore either a 1 in. image sensor must be used or a means of magnifying the image must be utilized. Several techniques were investigated such as: 1) the use of a high resolution 1 in. vidicon; 2) the use of optical magnification and a 2 in. vidicon; and 3) the use of a magnifying light intensifier coupled to a fiber optic input 2 in. vidicon. The present state-of-the-art for 1 in. vidicons makes it impossible to meet the desired resolution by this relatively simple solution. In view of this, our attentions were directed to those techniques utilizing a 2 in. vidicon as the image sensor. The use of a lens for a 2:1 optical magnification would appear to be an obvious solution; however, such is not the case. The "T" number of the optical probe coupled with the attenuation of the additional lens and associated 4:1 image area magnification, place an awesome burden on the model illumination to achieve a faceplate illumination of 1 ft lambert. In addition, due to the output characteristics of the Farrand probe, the lens must exhibit a resolution of 100 line pairs/ mm resolution at f/1.0 or better. While it may be possible to obtain such a lens, other solutions are more practical since we still have a significant illumination problem.

The technique which offered the highest resolution and least amount of difficulty to implement utilized an image magnifying light intensifier coupled to a 2 in. vidicon. In this configuration, the scene as viewed by the optical probe is imaged upon the input of the intensifier. The input image has a 16 mm diagonal at this point. The image is magnified within the image intensifier to a 32 mm diagonal and is intensified by a factor of 30:1. This matches the 35 mm usable diagonal of the 2 in. vidicon very nicely. The chief advantage of this technique over all others mentioned lies in the reduced number of optical or fiber optic elements contributing to the overall MTF. This is true even with the case involving the relay lens, since, in a practical configuration, an intensifier would be required to overcome the light losses in the optical system.

Radiometric and Photometric Research

As was mentioned previously, the goal of this program was optimization of all factors contributing to the quality of the video signal. Certainly one of the key components is the model decoration.

In order to conduct an effective evaluation, a model was constructed depicting an airfield with a variety of surrounding terrain ranging from marsh land, forested areas, farm land, to sand desert. The model paints and textures were selected to represent real earth colors and hues. Radiometric and photometric studies were conducted on the model, model illumination, the optical probe and the image intensifier. It is our opinion the most important conclusion reached as a result of the photometric and radiometric studies is that the model painting and decoration must be done under restraints imposed by the spectral response of the chosen model illumination, optical probe and image sensor. It was quite apparent from our investigation that, while the model appeared quite realistic to the human eye, the wide response of the image intensifier and general lack of blue response in the optical probe, caused a distinct loss of detail in the video image in some areas of the model. This was particularly noticeable during a simulated landing approach to the runway when it was difficult to discern the runway from the immediate background. It is our conclusion, therefore, that the model decoration should be physically implemented with the aid of a sensor having the spectral characteristics of the combined optical probe and image sensor, and under the chosen type of model illumination. This could be accomplished quite easily with an image intensifier, a lens, and a spectral filter exhibiting the spectral response of the optical probe. This would alleviate the problem of manipulating the entire optical probe/TV camera combination to view the model, and would even remove the requirement for this equipment during model construction.

Another important part of the study was in the area of model illumination. A through investigation of the spectral response, efficiency and usable life of incandescent, high pressure discharge and low pressure discharge illumination sources was conducted. Of those tested, the high pressure discharge lamps (sodium, metalarc and multivapor) were superior. In general the life is from 6000 to 16000 hr and efficiency is from 90 to 120 lumens/w with the sodium being the superior device in both catagories. Spectral response is a different matter however. The sodium emitts the majority of its energy between 550 and 650 nanometers. This is quite satisfactory for a monochrome system, however it would not be at all desirable for a color system. The metal-arc and multivapor lamps exhibit a very broad spectral response making them an excellent choice for color or monochrome systems.

2-In. Vidicon Camera Design

The key element in the achievement of a 2000 line resolution TV system is stability. This not only applies to the sync generator, but also to the sweep generators, deflection amplifiers, power supplies and video circuits. Much of the design effort associated with the camera development was to achieve the degree of stability required. Al-

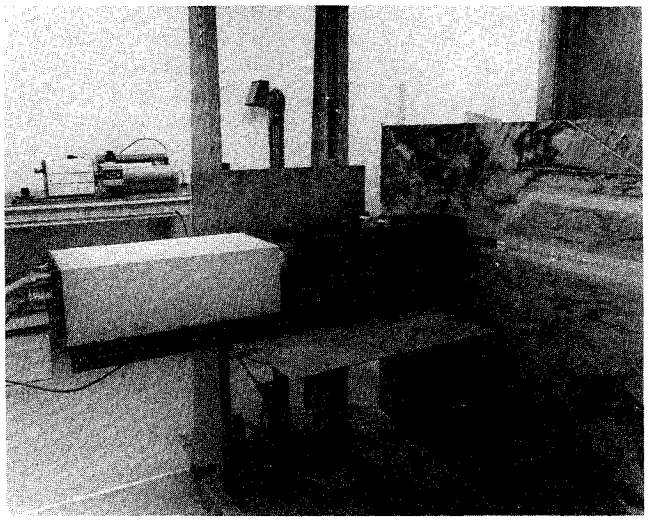

Fig. 1 TV system.

though all the signal generating circuitry employs feedback amplifiers which reject power supply changes, the power supplies for the camera utilize a two stage regulator for extreme stability over long periods of operation. This is especially important for systems operating at high line rates such as the 1365 lines per frame for which the camera was primarily designed.

Since the optical probe used with the camera introduces barrel distortions of the scene, the camera utilizes linear deflection amplifiers. This allows the raster to be shaped to correct for the optical distortions and any other symmetrical distortions due to slight imperfections in the yoke, vidicon, etc. Of course, since the vidicon is a velocity sensitive device, the raster shaping does cause a change in beam velocity, and the output signal amplitude is affected. To compensate for this change in amplitude, another correction signal is generated for use with the video amplifier which has a gain proportional to a DC voltage. Some of the other features exhibited by the camera are shading correction and dynamic focus. A deflection yoke of unique design was developed under this program to achieve nearly uniform resolution and extremely low beam landing error.

The video preamplifier and processor employed in this camera was required to achieve an absolute minimum of 60 MHz bandwidth in order to achieve the design goal of a 2000 element horizontal, 1000 element vertical system resolution. SRL had developed a 90 MHz video amplifier design in a previous development effort[2] which provided much valuable information. Using techniques discovered during the previous development effort, a new preamplifier was designed which has proven to be far superior to any known design, both from a bandwidth and signal-to-noise standpoint.

Camera Performance

The UHR 2 in. vidicon camera (Fig. 1) is capable of operation at any line rate from 525 to 1365 lines per 30 Hz frame, 2:1 interlace. In order to achieve the design goal of 2000 TV lines resolution horizontal and 1000 TV lines vertical for a 2:1 aspect ratio, all data was obtained while the system was operated at a line rate of 1365 lines per 30 Hz frame. Data was obtained using a Tektronix, Model 454 wideband DC to 150 MHz oscilloscope for selected line measurements of the video modulation. The data was recorded with an oscilloscope camera.

Figure 2a is a particularly good example of the resolving power of the camera. The photograph shows the 375, 750, and 1500 points on the resolution wedge. Close examination of the photograph will show that the camera is exhibiting 100% modulation through 750 lines and 50% modulation at 1500 TV lines.

Although the selected line technique is an excellent method of determining the resolution, signal-to-noise, and dynamic range of a television camera, many undesirable conditions are not easily discerned with this method. The effects of synchronized noise, poorly compensated high or low frequency response, damped oscillations, distortions, shading, etc. are far easier to observe on a television display. Photographs of various test patterns were taken with the use of an SRL Model 316-14 high resolution TV monitor.

The grey shade rendition of the camera is easily seen in Figure 2b, c, which shows the selected line photograph with full video bandwidth and with the 5 MHz bandwidth limiter on. Another interesting factor which can be seen on these photographs is the extremely good signal-to-noise ratio of the camera video amplifiers. Those persons familiar with wide bandwidth video systems will observe that the two photographs are a graphic demonstration of the signal-to-noise. It can be seen that most of the noise is above 5 MHz and therefore is not easily discerned in the displayed video image. It also should be noted that the noise represents less than one grey shade of the video waveform even on the full bandwidth photograph.

This program has shown that low noise, high resolution, real time video signals can be obtained from a 135° field of view optical probe and aircraft visual simulator terrain models. It has been reported that it is necessary that selection of the materials and processes to fabricate the terrain models be developed with consideration of the spectral characteristic of the TV sensor and the light sources if the grey scale rendition of the displayed image is to appear natural. With proper consideration to video hardware

Fig. 2a Signal modulation.

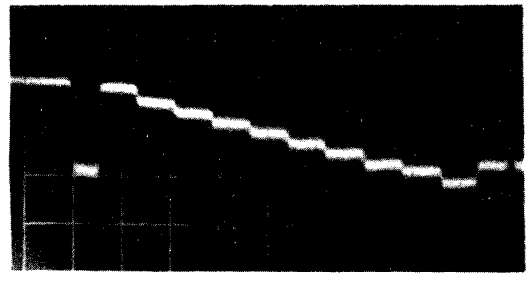

Fig. 2b Grey scale at full bandwidth.

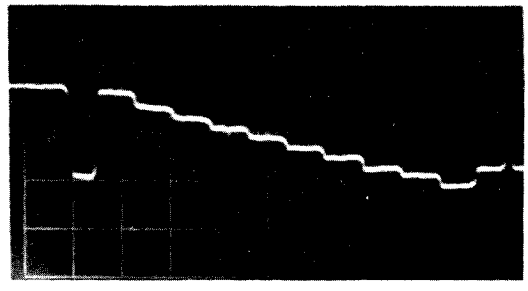

Fig. 2c Grey scale at 5MHz bandwidth.

development and the coordination of model makers art with the engineers talents, optimized video outputs from wide-angle infinite depth of focus optical probes can be achieved.

References

[1]Nagler, A. H. and Mazurkewitz, A. R., "Wide Angle Infinite-Depth-of-Field Optical Pickup for Visual Simulation," AFHRL-TR-71-41, Air Force Human Resources Lab., Wright-Patterson Air Force Base, Ohio.

[2]Mays, J. A., "The Development and Evaluation of a Ultra High Resolution Television System," AFHRL-71-1, Air Force Human Resources Lab., Wright-Patterson Air Force Base, Ohio.

Extension of a Vortex-Lattice Method to Include the Effects of Leading-Edge Separation

D. T. Mook* and S. A. Maddox†

Virginia Polytechnic Institute and State University, Blacksburg, Va.

Introduction

THE accurate determination of the aerodynamic characteristics of thin, highly swept wings having sharp leading edges at low, subsonic Mach numbers is a long-standing problem. The major difficulty stems from the fact that the flow separates from the wing along the leading edge, even for moderate angles of attack. Peckham[1] describes the actual flowfield. Maddox,[2] who reviewed the earlier attempts to model this separated flowfield, found that all of these attempts were analytical, and none resulted in accurate predictions of lift, pitching moment and pressure distribution.

Vortex-lattice methods have been used successfully to obtain the aerodynamic coefficients of lifting surfaces without leading-edge separation. In the present Note, we describe how an existing vortex-lattice method can be modified to include the effects of leading-edge separation and then use the modified version to calculate the aerodynamic loads on a highly swept delta wing. The present results are compared with Peckham's experimental data.

Description of the Method

The leading-edge vortex system is represented by a family of discrete vortex lines. Each line is composed of a series of straight segments joined head to tail. This system of discrete lines is superposed on the existing vortex-lattice system. The arrangement is illustrated in Fig. 1. Points A, B, and C lie on a typical vortex line in the leading-edge system. The semi-infinite segment from A to B is coincident with a leg of one of the horseshoe elements of the vortex lattice. The portion of the line between B and XMAX is composed of a series of short, straight segments; the lengths of these segments increase with the distance from B. The remaining semi-infinite segment from XMAX to C is straight and parallel to the undisturbed freestream velocity. As in the vortex-lattice method, the velocity field generated by the leading-edge system is calculated with the aid of the Biot-Savart law. This flowfield is added to that generated by the lattice and the free stream.

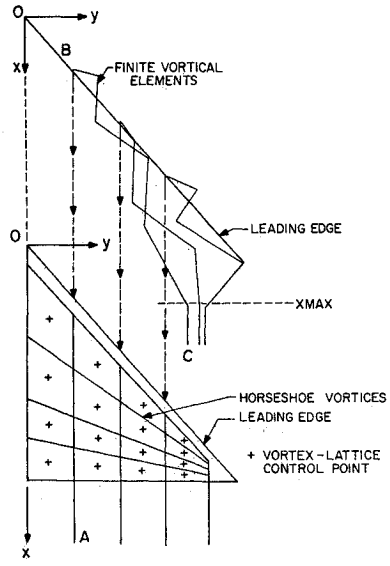

Fig. 1 Arrangement of discrete vortex lines.

Following Belotserkovskiy,[3] who considered wing-tip vortex systems and nonplanar wakes adjacent to the trailing edge, we make each of the segments between B and XMAX parallel to the velocity at its upstream end. This approximately renders each segment force free. A row of control points, one point for each line in the leading-edge vortex system, is added midway between the foremost spanwise elements of the lattice and the leading edge. Consequently, there is now a row of control points between the lattice and the leading as well as the trailing edge, and according to one of the basic notions of the vortex-lattice method, we are now satisfying a leading-edge as well as a trailing-edge Kutta condition.

Method of Solution

When the directions of the short, straight segments are specified, one can solve for the circulation around each vortex in the entire system by simultaneously satisfying

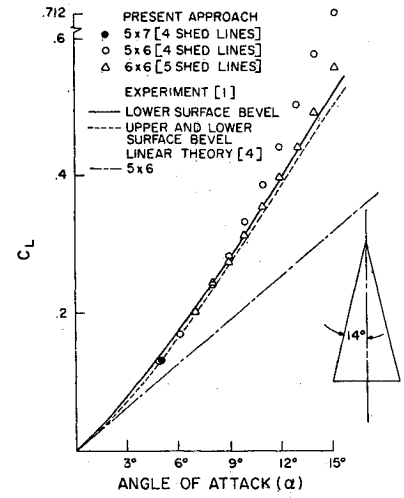

Fig. 2 Lift coefficient vs angle of attack.

Received August 8, 1973. Research sponsored by NASA Langley Research Center under Grant NGR-74-004-090. The authors acknowledge the numerous helpful comments and criticisms of Drs. A. H. Nayfeh, E. C. Yates, and W. P. Rodden.

Index category: Aircraft Aerodynamics.

*Associate Professor, Department of Engineering Science and Mechanics.

†Graduate Research Assistant, Department of Engineering Science and Mechanics.